frontiers | Frontiers in Cell and Developmental Biology

TYPE Original Research
PUBLISHED 02 November 2023
DOI 10.3389/fcell.2023.1247361

OPEN ACCESS

EDITED BY
Smadar Ben-Tabou De-Leon,
University of Haifa, Israel

REVIEWED BY
Philip Reno,
Philadelphia College of Osteopathic Medicine (PCOM), United States
Takanori Amano,
RIKEN BioResource Research Center (BRC), Japan
Takayuki Suzuki,
Osaka Metropolitan University, Japan

*CORRESPONDENCE
Tadashi Nomura,
tadnom@koto.kpu-m.ac.jp
tadnom@kit.ac.jp

RECEIVED 26 June 2023
ACCEPTED 12 October 2023
PUBLISHED 02 November 2023

CITATION
Agata A, Ohtsuka S, Noji R, Gotoh H, Ono K and Nomura T (2023), A Neanderthal/Denisovan GLI3 variant contributes to anatomical variations in mice.
Front. Cell Dev. Biol. 11:1247361.
doi: 10.3389/fcell.2023.1247361

A Neanderthal/Denisovan GLI3 variant contributes to anatomical variations in mice

Ako Agata[1], Satoshi Ohtsuka[2], Ryota Noji[1], Hitoshi Gotoh[1], Katsuhiko Ono[1] and Tadashi Nomura[1,3]*

[1]Developmental Neurobiology, Kyoto Prefectural University of Medicine, Kyoto, Japan, [2]Laboratories for Experimental Animals, Kyoto Prefectural University of Medicine, Kyoto, Japan, [3]Applied Biology, Kyoto Institute of Technology, Kyoto, Japan

Changes in genomic structures underlie phenotypic diversification in organisms. Amino acid-changing mutations affect pleiotropic functions of proteins, although little is known about how mutated proteins are adapted in existing developmental programs. Here we investigate the biological effects of a variant of the GLI3 transcription factor (GLI3^{R1537C}) carried in Neanderthals and Denisovans, which are extinct hominins close to modern humans. R1537C does not compromise protein stability or GLI3 activator-dependent transcriptional activities. In contrast, R1537C affects the regulation of downstream target genes associated with developmental processes. Furthermore, genome-edited mice carrying the Neanderthal/Denisovan GLI3 mutation exhibited various alterations in skeletal morphology. Our data suggest that an extinct hominin-type GLI3 contributes to species-specific anatomical variations, which were tolerated by relaxed constraint in developmental programs during human evolution.

KEYWORDS

Gli3, Neanderthals, Denisovans, skeletal development, evolution

Introduction

Understanding the genetic mechanisms underlying phenotypic variation is a fundamental challenge in developmental and evolutionary biology. Several empirical studies suggest that adaptive mutations occurring in *cis*-regulatory regions are a major force driving morphological evolution (Carroll, 2000; Chan et al., 2010; Werner et al., 2010; Kvon et al., 2016). In contrast, mutations in protein-coding regions have been thought to play little role in anatomical variations, since structural mutations often disrupt protein function and cause severe malformations or pathological conditions in organisms. However, recent studies have revealed that changes in protein structures result in novel pleiotropic functions (Ronshaugen et al., 2002; Protas et al., 2006; Hoekstra and Coyne, 2007). Thus, nucleotide variants that alter amino acid sequences contribute significantly to phenotypic diversity.

Adaptive mutations in coding regions are behind the phenotypic diversifications in human evolution as well (Cargill et al., 1999; Chasman and Adams, 2001; Enard et al., 2002; Asgari et al., 2020). Accumulating data have shown that several admixtures resulted in gene flow between modern human ancestors and archaic hominins such as Neanderthals and Denisovans, who diverged from modern humans approximately 520–630 thousand years ago (Prufer et al., 2014; Prufer et al., 2017). Fossil evidence has indicated distinct anatomical characteristics in Neanderthals compared to modern

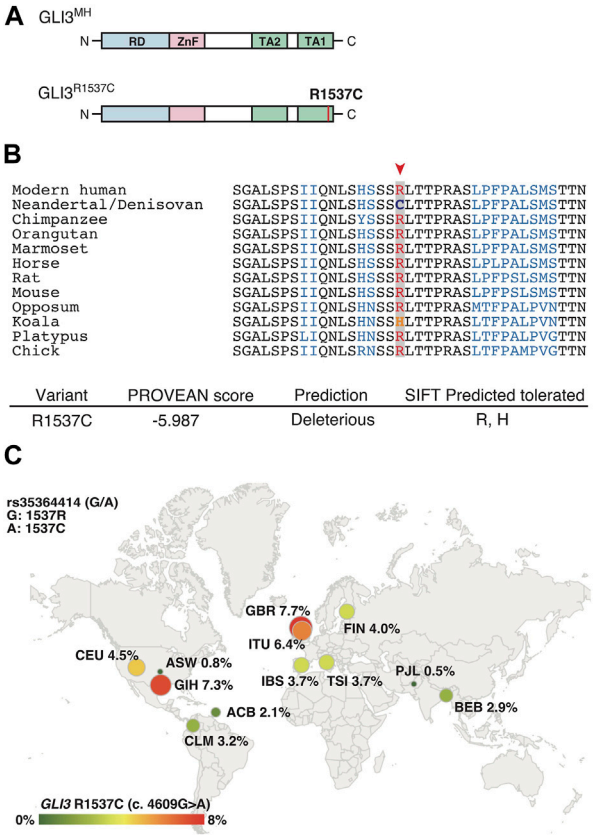

FIGURE 1
GLI3^{R1537C} is a derived mutation in archaic and present-day humans **(A)** Protein structures of the modern human GLI3 (GLI3^{MH}) and a Neanderthal and Denisovan GLI3 variant (GLI3^{R1537C}). RD, repressor domain; ZnF, Zinc finger type DNA binding domain; TA1, transactivation domain 1; TA2, transactivation domain 2. **(B)** Upper panel: amino acid sequences of GLI3/Gli3 C-terminal regions in mammals and a bird (chick). A red arrowhead indicates the corresponding arginine position. Lower panel: PROVEAN score and SIFT prediction of GLI3^{R1537C}. **(C)** Allele frequencies of R1537C (rs35364414; A allele) in 1000G populations. ACB, African Caribbean in Barbados; ASW, African ancestry in Southwest US; CLM, Colombian in Medellin, Columbia; CEU, Utah residents with Northern and Western ancestry; FIN, Finnish in Finland; GBR, British in England and Scotland; IBS, Iberian population in Spain; TSI, Toscani in Italy; BEB, Bengali in Bangladesh; GIH, Gujarati Indian in Houston; ITU, Indian Telugu in the UK; PJL, Punjabi in Lahore, Pakistan.

humans, including elongated and low crania, larger brow ridges, and broader rib cages (Reilly et al., 2022). Putative morphological profiles inferred from DNA methylation patterns predict that Denisovans may have shared some Neanderthal traits (Gokhman et al., 2019). Some of the genetic diversity of extant humans is derived from the extinct hominins (Green et al., 2010; Meyer et al., 2012; Prufer et al., 2014; Sankararaman et al., 2016; Skov et al., 2020). Recent studies have unveiled some of the functional consequences of coding variations specific to archaic or modern humans (Zeberg et al., 2020; Greer et al., 2021; Maricic et al., 2021; Trujillo et al., 2021; Mora-Bermudez et al., 2022; Pinson et al., 2022). However, the impact of archaic genomic variants in anatomical structures has not been directly demonstrated.

Previous studies have revealed that relative to modern humans, all sequenced Neanderthals and Denisovans carry an amino acid substitution in the C-terminal region of GLI3 (R1537C) (Castellano et al., 2014; Prufer et al., 2014). GLI3 is a GLI-Krüppel family transcription factor that plays essential roles in embryonic development by mediating Hedgehog signaling (Matissek and Elsawa, 2020). In the absence of Hedgehog, GLI3 is cleaved to form the N-terminal repressor form, while the presence of Hedgehog prevents protein processing, which triggers intracellular accumulation of full-length GLI3. Functional disruptions of GLI3 normally result in severe abnormalities in various anatomical structures in mice and humans (Vortkamp et al., 1991; Kang et al., 1997; Naruse et al., 2010). R1537C variant of GLI3 corresponds to a single nucleotide polymorphism (SNP) that exists in modern human populations (rs35364414, 4609G>A results in arginine to cysteine substitution). However, the consequences of the amino acid substitution of the GLI3 protein and phenotypic outcomes have not been clarified.

Here, we investigated the biological effects of the Neanderthal/Denisovan GLI3 variant (R1537C). Our study shows that R1537C substitution affects the regulation of downstream target genes associated with developmental processes without interfering Hedgehog-dependent transcriptional activities. Genome-edited mice carrying the Neanderthal/Denisovan GLI3 mutation exhibited various alterations in skeletal morphology depending on genetic backgrounds. The data suggest that the extinct hominin-type GLI3 variant affects species-specific anatomical variations, which were accommodated by concurrent changes in developmental constraints during human evolution.

Results

The R1537C variant might be accommodated in archaic and modern humans

R1537C is localized at C-terminal transactivation domain 1 (TA1) of human GLI3 (Figure 1A). At this position, arginine (R) is extensively conserved among mammals and a bird (Figure 1B), suggesting that the corresponding cysteine residue is a derived mutation in Neanderthal/Denisovan lineages. *In silico* analysis of protein functions predicted that R1537C is deleterious to human GLI3 (Figure 1B). Of note, the SIFT program suggested that substitution to histidine was tolerable at this position, which corresponds to the altered amino acid in Koala Gli3 (Figure 1B). These data suggest that relaxed constraint on the residue occurred in the evolution of archaic human lineages. Next, we investigated the R1537C variant exists in modern human population. Present-day human genomes outside Africa contain 1%–4% DNA derived from Neanderthals, while approximately 6% of the Melanesian genomes are derived from Denisovans (Green et al., 2010; Reich et al., 2010). We checked geographic distribution of the SNP corresponding to the R1537C variant in the modern human population [rs35364414 (G/A)]. The allele frequency of the R1537C variant (A allele) ranges from highest in the European population (3.7%–7.7%) to lowest in the African population

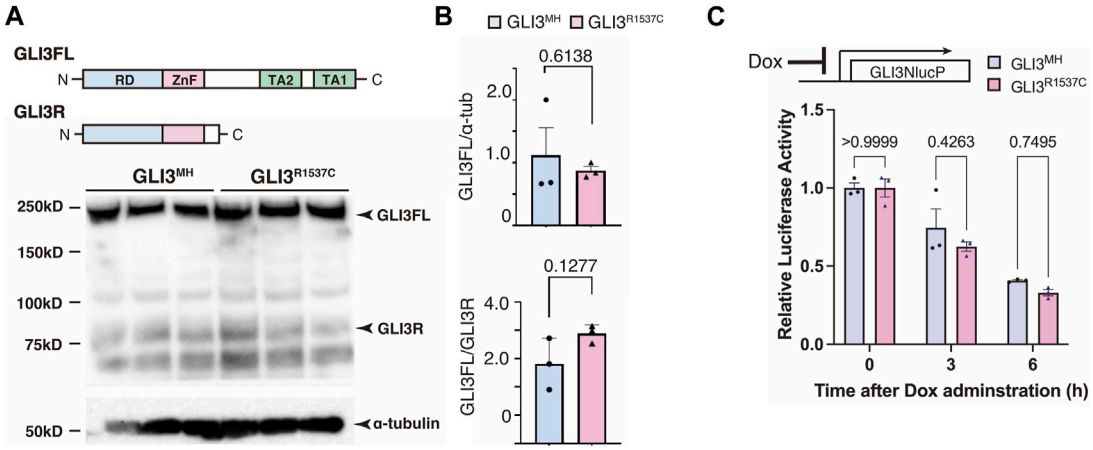

FIGURE 2
R1537C does not compromise GLI3 protein stability **(A)** Western blotting of GLI3^{MH} and GLI3^{R1537C}. **(B)** Quantification of GLI3FL (full length, upper panel) and GLI3FL/GLI3R ratio (lower panel). **(C)** Comparison of the degradation speed of nanoluc (NlucP)-tagged GLI3^{MH} and GLI3^{R1537C} after halting protein synthesis by doxycycline administration.

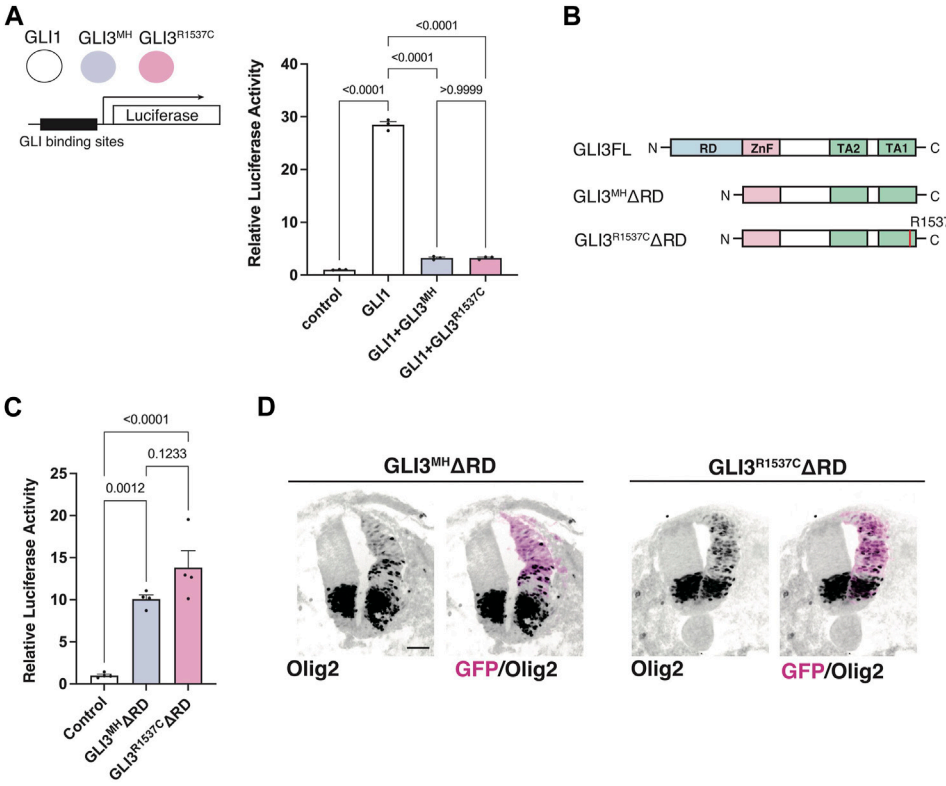

FIGURE 3
R1537C does not interfere repressor or activator-dependent transcriptional activities **(A)** GLI-reporter activities in HEK293T cells overexpressing GLI3^{MH} or GLI3^{R1537C} together with GLI1. **(B)** Protein structures of full-length and repressor domain-truncated GLI3 (GLI3^{MH}ΔRD or GLI3^{R1537C}ΔRD). **(C)** GLI-reporter activities in HEK293T cells overexpressing GLI3^{MH}ΔRD or GLI3^{R1537C}ΔRD. **(D)** Induction of Olig2 expression in the developing chick neural tube by overexpression of GLI3^{MH}ΔRD or GLI3^{R1537C}ΔRD. Scale bar: 50 μm **(D)**.

(0.8%–2.1%) (The 1000G genome dataset, Figure 1C). A previous study suggested that the chromosomal fragment containing the SNP was inferred to be derived from archaic hominins (Skov et al., 2020). These lines of evidence suggest that the R1537C variant is accommodated in genetic background of archaic and present-day humans.

The R1537C variant does not compromise protein stability and Hedgehog-dependent GLI3 functions

Next, we investigated whether R1537C substitution affects GLI3 protein expression. To test this, we overexpressed modern human-type GLI3 ($GLI3^{MH}$) or a Neanderthal/Denisovan GLI3 ($GLI3^{R1537C}$) in human embryonic kidney cells (HEK293T cells) and performed Western blotting. The amounts of full-length and truncated forms of GLI3 (GLI3 full and GLI3R, respectively) were comparable between $GLI3^{MH}$ and $GLI3^{R1537C}$ (Figures 2A, B). Specificity of the GLI3 antibody was confirmed by Western blotting with GLI3 KO cell lines (Supplementary Figures S1A–C). To further examine the stability of $GLI3^{MH}$ and $GLI3^{R1537C}$, we overexpressed luciferase tagged $GLI3^{MH}$ and $GLI3^{R1537C}$ and measured luciferase activity after halting protein expression. We confirmed that the degradation rate was not different between of $GLI3^{MH}$ and $GLI3^{R1537C}$ (Figure 2C). Thus, in contrast to *in silico* prediction, R1537C substitution does not disturb the protein stability of GLI3.

Next, we test whether R1537C substitution affect GLI-mediated Hedgehog signaling. Previous studies reported that full-length GLI3 predominantly acts as an inhibitor of Hedgehog signaling, as GLI3 negatively regulates GLI1-dependent transcriptional activity (Wang et al., 2000). Thus, we examined the effect of R1537C on the suppressive potential of GLI3 in the presence of GLI1. To test this, we overexpressed a GLI reporter vector together with GLI1 and $GLI3^{MH}$ or $GLI3^{R1537C}$ in HEK293T cells (Figure 3A). Compared to the control, GLI1 strongly enhanced reporter activity, while co-transfection of $GLI3^{MH}$ or $GLI3^{R1537C}$ significantly decreased GLI1-dependent reporter activity, indicating that the repressive activity of GLI3 is not curtailed by the amino acid substitution.

Full-length GLI3 contains both transcriptional repressor and activator domains. To directly assess the effect of R1537C on the transcriptional activator domain, we removed the N-terminal repressor domain and examined luciferase activity in response to GLI3 variants ($GLI3^{MH}\Delta RD$ and $GLI3^{R1537C}\Delta RD$, Figure 3B). Compared to the control, both $GLI3^{MH}\Delta RD$ and $GLI3^{R1537C}\Delta RD$ significantly increased reporter activity at comparable levels (Figure 3C). Furthermore, we corroborated that overexpression of $GLI3^{MH}\Delta RD$ and $GLI3^{R1537C}\Delta RD$ induced the expression of Olig2, a direct downstream target of GLI proteins, in the developing chick neural tube (Figure 3D). These data indicate that R1537C does not affect the function of transcriptional activator domain of GLI3.

R1537C affects unique downstream gene expression related to anatomical structures

Our luciferase assay suggest that R1537C preserves transcriptional activity of GLI3. To elucidate the impact of R1537C on GLI3-dependent unique target genes, we overexpressed full-length $GLI3^{MH}$ or $GLI3^{R1537C}$ in HEK293T cells and performed RNA sequencing (RNA-seq) analysis. Because GLI3 is weakly expressed in HEK293T cells, we also performed RNA-seq with control HEK293T cells transfected with empty vector to capture background level of gene expression. First, we checked the expression of direct downstream genes of Hedgehog signaling, such as *NKX2.2*, *NKX6.1*, *PAX6*, *IRX3*, and *OLIG2*. Compared to the control, these genes were slightly up- or downregulated by full-length GLI3 overexpression. Importantly, we could not detect differences in Fold change (Fc) of these genes between $GLI3^{MH}$ and $GLI3^{R1537C}$ overexpression (Figure 4A), corroborating that R1537C does not interfere with Hedgehog-dependent signaling. Next, we focused on differentially expressed genes [DEGs; $|Fc| \geq 1.5$, false discovery rate (FDR) < 0.05] between the control and $GLI3^{MH}$ or $GLI3^{R1537C}$ overexpression. Compared to the control HEK293T cells, a total of 846 and 671 genes were differentially expressed by the overexpression of $GLI3^{MH}$ or $GLI3^{R1537C}$, respectively (Supplementary Table S1). We further conducted Gene Ontology (GO) enrichment analysis to identify the functional characteristics of DEGs. Compared to control, $GLI3^{MH}$ overexpression enriched GO terms related to various biological processes, consistent with the pleiotropic functions of GLI3. Specifically, $GLI3^{MH}$ overexpression enriches GO terms associated with developmental process, such as ossification, renal system development, and extracellular matrix organization (Figure 4B). In contrast, $GLI3^{R1537C}$ did not enriched these GO terms, but increased terms related to chromatin and nucleosome assembly (Figure 4B). To further investigate altered gene regulations by R1537C, we directly compared transcriptomes with $GLI3^{MH}$ and $GLI3^{R1537C}$ overexpression and identified 91 DEGs that were significantly up- or downregulated by $GLI3^{R1537C}$ (DEGs in $GLI3^{R1537C}$ vs. $GLI3^{MH}$; $|Fc| \geq 1.5$, FDR < 0.05, Supplementary Table S2). These DEGs included unique transcripts, such as LINC00294, a human specific noncoding RNA that is involved in cell proliferation (Qiu et al., 2020; Zho et al., 2020; Dong et al., 2021), and *SLC9A3* (NHE3), a member of the sodium-hydrogen exchanger family that is responsible for the maintenance of sodium balance (Orlowski and Grinstein, 1997). Among them, 23 genes were associated with developmental process (Figure 4C). Notably, H4 clustered histone 3 (*H4C3*; Fc = 3.7935, $p = 0.0465$) plays an essential role in chromatin organization and disruption of this gene results in growth retardation and skeletal abnormalities in humans (Tessadori et al., 2022). Stanniocalcin 1 (*STC1*; Fc = −2.93183, $p = 7.15551E-05$) is a glycoprotein involved in calcium and phosphate metabolism, and *STC1* transgenic mice exhibited dwarf phenotype due to altered osteogenesis (Filvaroff et al., 2002). These data suggest that the missense mutation of GLI3 alters transcriptional regulations related to specific organ development during embryogenesis.

Mice with a Neanderthal/Denisovan-type Gli3 variant exhibit altered skeletal morphology

To further characterize the effect of R1537C on embryonic development, we created knock-in mice with the Neanderthal/Denisovan GLI3 variant by CRISPR-mediated genome engineering technology. In mice, the amino acid that corresponds to the missense variant is naturally arginine (1540R) (Figures 1A, 5A). Thus, we introduced the point mutation c4618t by Cas12 (Cpf1)-dependent homologous recombination, resulting in an R1540C substitution in the mouse GLI3 protein (Figure 5B, Supplementary Figures S2A–C). Western blotting in HEK293T cells confirmed that the amino acid substitution did not compromise protein expression compared to wild type GLI3 (1540R) (Supplementary Figure S2D). On the

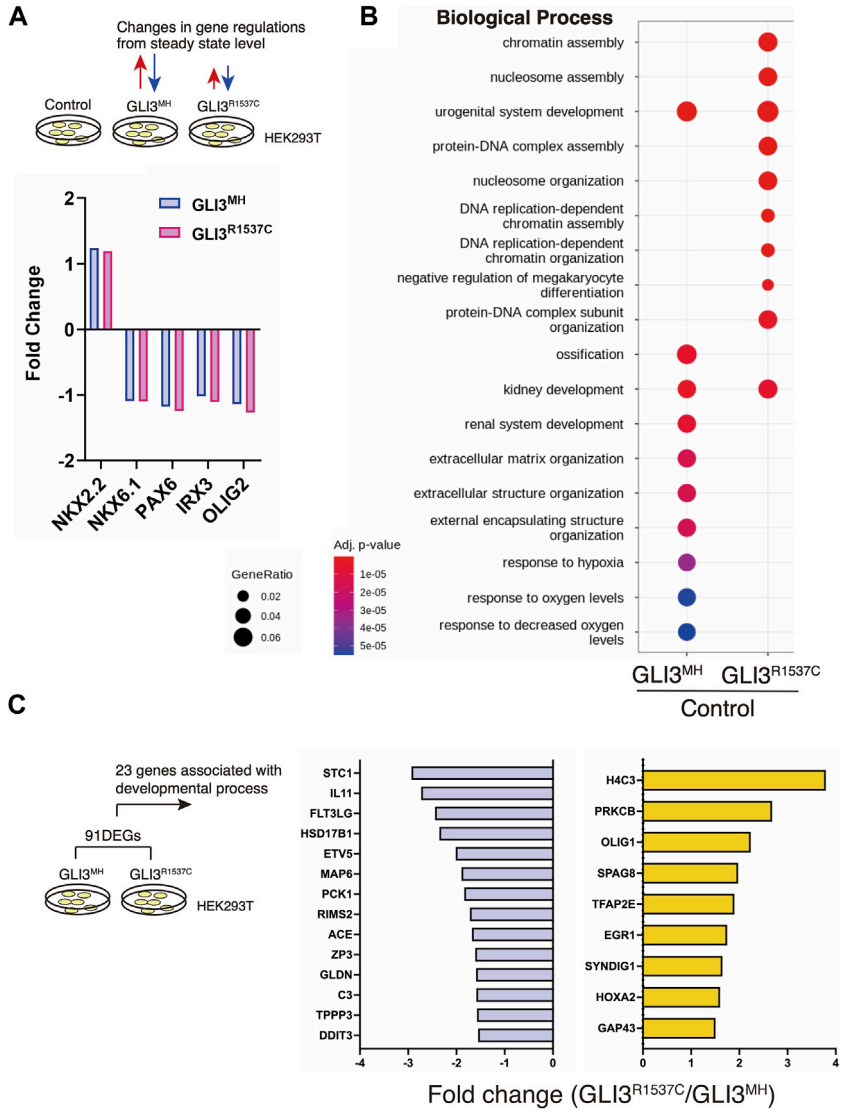

FIGURE 4
R1537C alters the regulation of GLI3-dependent gene expression **(A)** Fold changes of direct downstream genes of Hedgehog signaling in HEK293T cells overexpressing $GLI3^{MH}$ or $GLI3^{R1537C}$ compared with control samples. **(B)** GO enrichment analysis in comparisons of HEK293T cells overexpressing $GLI3^{MH}$ or $GLI3^{R1537C}$ versus control samples. Spots represent the top-ranking terms with gene ratios over 0.02. **(C)** Genes associated with developmental process that were down- or upregulated by $GLI3^{R1537C}$ compared with $GLI3^{MH}$ overexpression.

C57BL6 background, mice carrying 1540C were born at the expected Mendelian ratio. Both full-length and repressor form of Gli3 were detected in homozygous 1540C/1540C mice as well as heterozygous (1540R/1540C) and wild-type mice (Figure 5C), corroborating that protein processing is not impaired in the Gli3 variant. Homozygous 1540C mice had similar body sizes to wild type or heterozygous (1540R/1540C) littermates (Supplementary Figure S2E). However, we observed altered head morphology in 1540C homozygous mice compared with the wild type or heterozygous littermates. Whole mount skeletal analysis indicated enlarged crania with frontal and parietal bossing in the 1540C mice (Figures 5D, G and Supplementary Table S3). Previous studies reported that Gli3 null mice (*Gli3*$^{xt/xt}$) exhibited craniosynostosis, a premature closure of cranial sutures, which frequently results in abnormal shape of skulls (Veistinen et al., 2012). Consistently, deformed skulls in 1540C mice were frequently associated with premature ossification at the coronal suture (Figures 5E, F).

Some homozygous 1540C mice exhibited asymmetric shapes of rib cages associated with scoliosis (Figure 5H and Supplementary Table S3). Furthermore, compared to wild type mice, the number of lumbar vertebrae was reduced in heterozygous and homozygous mice carrying the 1540C allele (Figure 5I and Supplementary Table S3). Polydactyly was shown to be a typical phenotype caused by Gli3/GLI3 null conditions in both mice and humans (Naruse et al., 2010). In contrast, the heterozygous and homozygous 1540C mice did not exhibit any abnormalities in limb and digit formation (Supplementary Figure S2E). These results indicated that a Neanderthal/Denisovan Gli3 variant resulted in altered skeletal morphology, which differed from the phenotypes associated with the loss of Gli3 functions.

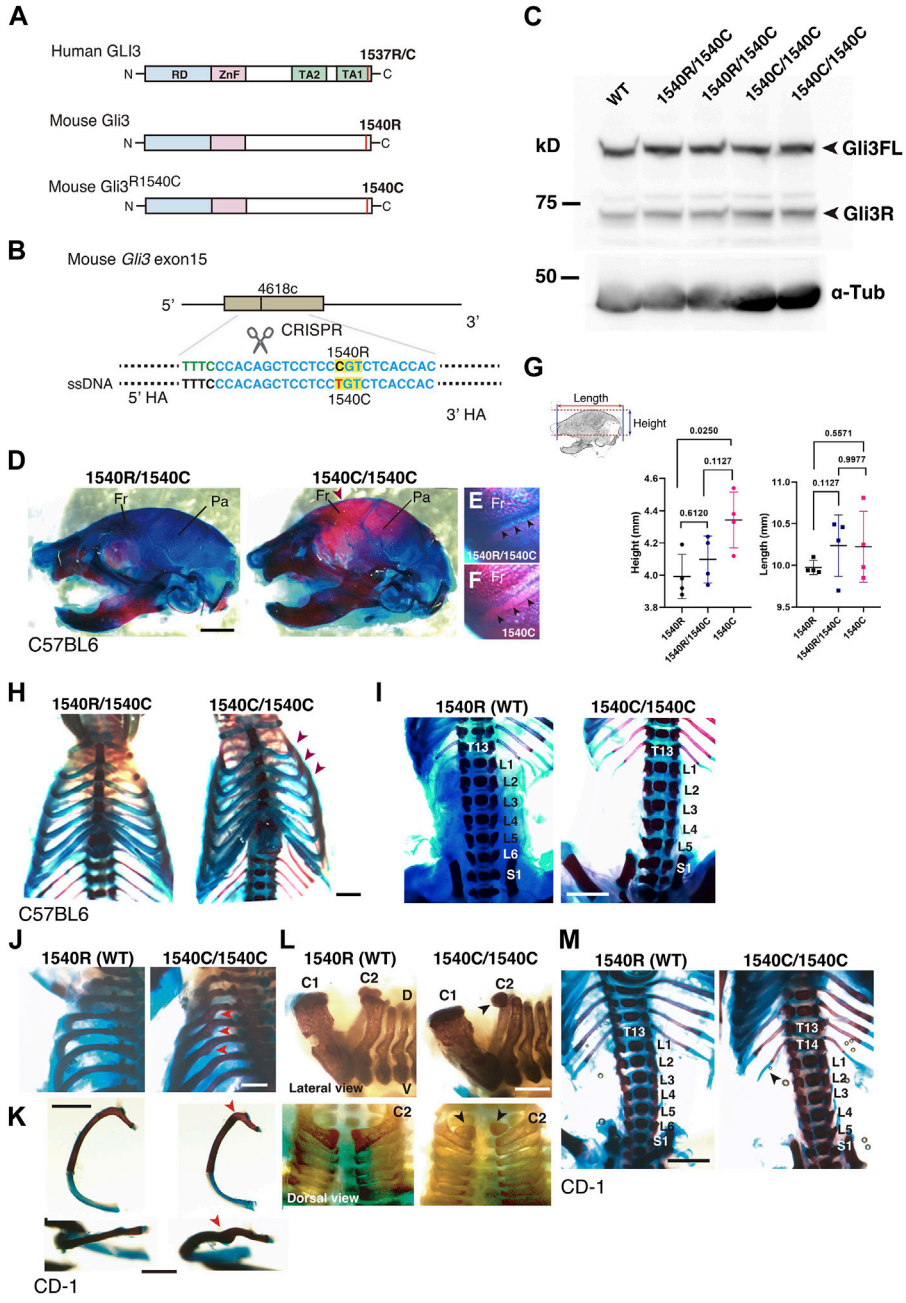

FIGURE 5
Altered skeletal morphology of the mice carrying a Neanderthal/Denisovan type GLI3 variant **(A)** Structures of modern human or extinct hominins GLI3, wild type mouse Gli3 ($Gli3^{1540R}$), and mouse Gli3 with a Neanderthal/Denisovans variant ($Gli3^{1540C}$). **(B)** Single nucleotide substitution in mouse Gli3 by CRISPR-mediated genome editing. **(C)** Western blotting of wild-type (WT), heterozygous (1540R/1540C) and homozygous (1540C/1540C) mouse brains (E17.5 cerebellar primordium) with anti-GLI3 antibody. **(D–F)** The skull of heterozygous (1540R/1540C) and homozygous (1540C/1540C) mice on C57BL6 background. An arrowhead indicates an enlarged cranium in 1540C mouse. **(E,F)** Coronal sutures (arrowheads) of heterozygous **(E)** and homozygous **(F)** mice. **(G)** Quantification of skull height and length. **(H)** Comparison of rib cages. Arrowheads indicate abnormal rib torsion in 1540C/1540C mice. **(I)** Reduced number of lumber vertebrae in 1540C/1540C mouse. **(J–M)** Skeletal morphology of mice on CD-1 background. The 1540C/1540C mice exhibit a twist of the posterior angle of the rib [arrowheads in **(J,K)**], hypoplastic ossification in the 2nd cervical vertebrae [arrowheads in **(L)**], extra thoracic ribs [T14, arrowheads in **(M)**] and reduced number of lumber vertebrae **(M)**. Scale bars: 1 mm.

It has been shown that calvarial ossification is mediated by Indian hedgehog (Ihh)-dependent signaling (Veistinen et al., 2017). To ask whether ossification phenotypes in 1540C mice is due to altered Ihh signaling, we examined the expression of *Ptch1*, a Hedgehog responsive gene, in the developing cartilage. We confirmed that *Ptch1* expression in the developing calvarial or thoracic mesenchymal tissues was comparable between wild type and 1540C homozygous mice (Supplementary Figures S3A–E), suggesting that altered ossification in 1540C mice was not due to dysregulation of Ihh signaling.

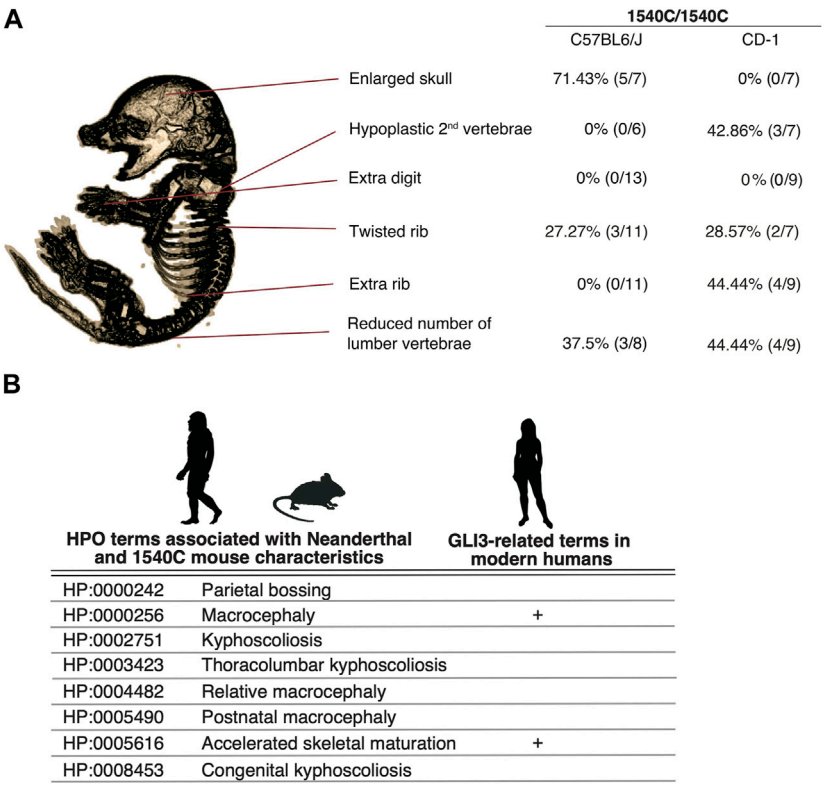

FIGURE 6
The arginine to cysteine substation in GLI3/Gli3 affects common anatomical structures in human and mice **(A)** Variation of skeletal phenotypes in $Gli3^{R1540C}$ mice on different genetic background. The proportion represents phenotypes in homozygous mice. **(B)** HPO terms shared with Neanderthal (Gokhman et al., 2020) and $Gli3^{R1540C}$ mouse anatomical characteristics. GLI3 related clinical features in modern humans are also represented. Images of Neanderthal, mouse and human are from PHYLOPIC.

Several lines of studies on archaic human genomes indicated that Neanderthals and Denisovans had distinct genetic backgrounds compared to modern humans, although these extinct hominins and ancestral modern humans had frequently intermixed with each other (Green et al., 2010; Meyer et al., 2012; Prufer et al., 2014; Reilly et al., 2022). Accordingly, the phenotypic consequences caused by the missense variant might be variable depending on specific genetic backgrounds. To examine this possibility, we introduced the 1540C substitution into mice with a CD-1 (ICR) background, which is an outbred strain with heterogeneity of individual genomic sequences compared to inbred strains. Homozygous 1540C mice were viable and their body sizes were similar to those of wild-type or heterozygous knock-in mice (Supplementary Figures S2F–H). As in the case of the knock-in mice on the C57BL6 background, CD-1 mice carrying the 1540C allele exhibited abnormal rib torsion (Figures 5J, K). In particular, the posterior angle of the ribs in 1540C mice was abnormally kinked, which resulted in the crank-shaft sternum (Figure 5K, Supplementary Figure S2I and Supplementary Table S3). Furthermore, we found additional phenotypes in CD-1 background mice, such as hypoplasia of the second cervical vertebrae and extra ribs at the 14th thoracic vertebrae (Figures 5L, M). The number of lumber vertebrae was reduced in the mice with extra ribs (Figure 5M). These skeletal abnormalities were also observed in a lower proportion of the heterozygous mice, indicating a dose-dependency of the phenotypes correlated with the presence of the 1540C allele (Supplementary Table S3). Curiously, extra 14th ribs occurred in a small proportion of the wild-type CD-1 mice (Supplementary Table S3), suggesting that the missense Gli3 variant increased phenotypic variations sustained in the background population. In contrast to C57BL6 background, cranial abnormalities were not detected in the homozygous mice on CD-1 background, suggesting that these phenotypes are highly affected by genetic background (Figure 6A).

Similarities in human and mouse transcriptomes depending on the GLI3/Gli3 variants

To identify downstream genes affected by the missense Gli3 variant in mice, we isolated mesenchymal tissues of wild-type and 1540C mouse embryos on the C57BL6 background and performed RNA-seq analysis. A total of 453 and 238 genes were up- or downregulated in 1540C compared to wild-type mice [|Fc| ≥ 1.5, false discovery rate (FDR) < 0.05, Supplementary Table S4]. We found that DEGs included *Msx1*, *Dlx1* and *Dlx2*, which were known to be essential for skeletal morphology (Alappat et al., 2003; Levi et al., 2022). Notably, several histone H4 cluster genes, such as *H4c2*, *H4c6* and *H4c14* were upregulated in 1540C mice, suggesting that the arginine to cysteine substitution of Gli3 commonly affects

specific histone components in mice and humans (Supplementary Table S4). To further address the commonalities of downstream target genes affected by the GLI3^{R1537C} and Gli3^{R1540C}, we compared the GO terms of HEK293T cells transfected with human GLI3 variants (Figure 4) and Gli3 knock-in mice. Although these data sets were derived from distinct species and cell types, the terms for cellular components showed remarkable similarity to the top-ranking enriched terms, including CENP-A-containing chromatin and CENP-A-containing nucleosomes (Supplementary Figures S4A, B). These results suggest that the missense variant of GLI3/Gli3 disturbed common downstream targets associated with nucleosome and chromatin assembly between human and mice.

The arginine to cysteine substation in GLI3/Gli3 affects common anatomical structures in human and mice

We demonstrate that mice with a Neanderthal/Denisovan GLI3 variant exhibit altered skeletal structures, such as enlarged cranium, altered shapes of vertebrae, and rib malformations (Figure 6A). As shown in Figure 6A, enlarged skull phenotype showed higher penetrance in C57BL6 mice, while such phenotype was not observed in CD-1 background mice. In contrast, hypoplastic vertebrae and extra ribs frequently occurred in CD-1 background mice, despite these phenotypes represented lower penetrance.

A recent study reported the association of unique anatomical phenotypes in Neanderthal with Human Phenotypic Ontology (HPO), a database of disease-associated human phenotypes (Gokhman et al., 2020). Notably, some of neanderthal-specific HPO phenotypes, such as macrocephaly (HP: 0000256), accelerated skeletal maturation (HP: 0005616) and kyphoscoliosis (HP: 0002751) are linked with the phenotypes of R1540C mice (Figure 6B and Supplementary Table S5). We find that the mice carrying the Neanderthal/Denisovan GLI3 variant also showed altered shapes of rib cages due to abnormal rib torsion (Figures 5H, J, K, 6A). Fossil evidence indicated a stronger torsion of central ribs (6th–8th ribs) in Neanderthal infants, which contributes to distinct rib cages (shorter and deeper forms) compared to those of modern humans (Garcia-Martinez et al., 2020). Even if not all skeletal phenotypes of R1540C mice phenocopied anatomical characteristics of extinct humans, phenotypic alterations in the knock-in mice suggest that the corresponding missense mutation of GLI3 might affect conserved developmental processes of homologous skeletal structures between mice and humans.

Discussion

Here, we show that an extinct hominin-specific amino acid alters GLI3 functions by conferring differential transcriptional regulation of downstream genes and results in altered skeletal morphology in mice. Several studies have shown that the ratio of GLI3 activator versus repressor is critical for mediating Hedgehog-dependent signaling during embryogenesis (Wang et al., 2007; Wen et al., 2010). Despite *in silico* prediction, we demonstrate that R1537C substitution does not compromise GLI3 protein stability or activator-dependent transcriptional activity. Furthermore, R1537C does not alter the regulations of direct target genes of Sonic hedgehog signaling. Thus, GLI3^{R1537C} does not interfere with the potential to mediate Hedgehog signaling during embryogenesis, thereby detouring deleterious phenotypes. In contrast, disruption of the GLI3 C-terminal region causes the pathogenic phenotypes in human (Demurger et al., 2015), suggesting that the C-terminal region is a prerequisite for GLI3 functions, possibly through interaction with various cofactors for transcriptional regulation (Zhou et al., 2006).

We also demonstrate that GLI3^{R1537C} affects the transcription of various nucleosome components, providing first evidence on the association of C-terminus region of GLI3 on chromatin assembly. Furthermore, transcriptome analysis of GLI3^{R1540C} knock-in mice revealed evolutionary conservation of these regulatory pathways between human and mice. It has been shown that *de novo* missense variants of histone H4 clusters results in various neurodevelopmental and skeletal abnormalities (Tessadori et al., 2022). Notably, a part of these clinical features, such as craniosynostosis, hypertelorism and syndactyly, are also reported in patients with *GLI3* variants (Vortkamp et al., 1991; Kang et al., 1997; Demurger et al., 2015). Although empirical data explaining the relationship between these pathways and developmental phenotypes are still limited, these lines of evidence suggest that phenotypic alterations by the GLI3 variant is mediated by global consequences of chromatin organization.

The corresponding amino acid substitution is highly unique in archaic hominins and modern humans. Various skeletal abnormalities induced by archaic hominin-type substitution might not be adaptive in mice. These lines of evidence suggest that concurrent changes in developmental programs occurring in archaic hominins accommodated R1537C-dependent phenotypic abrogation. Alternatively, the variant-dependent functional alterations might be tolerated by additional compensatory mutations that occurred in archaic and modern human lineages. R1537C-dependent phenotypes could be attributed to the interaction with other variants reside in archaic and modern human-specific genetic backgrounds. We confirmed that differential genetic background significantly affects Gli3 variant-dependent phenotypic variations in mice. Phenotypic differences might be due to genetic and/or epigenetic differences in other genomic regions, which affect Gli3-dependent developmental processes. Notably, the R1540C variant frequently contributed to 14th rib formation in CD-1 background, which also occurs occasionally in wild type population. It has been reported that variable number of vertebrae depends on genetic backgrounds as well as maternal influences (Mc and Michie, 1958; Rengasamy and Padmanabhan, 2004). A recent study reported that the R1537C variant is associated with neural tube defects in European population (Renard et al., 2019). Thus, it is possible that the GLI3^{R1537C}/Gli3^{R1540C} increase susceptibility to variable morphological characteristics or pathogenic phenotypes in response to genetic and environmental perturbations.

It remains unclear if R1537C variant was fixed in extinct hominin groups by positive selection. Recent studies have suggested that the small population size of Neanderthals was not effective for natural selection, by which weakly deleterious mutations might be accumulated by genetic drift (Prufer et al., 2014; Prufer et al., 2017). Notably, datasets of associations between various human traits and variants based on UK Biobank cohorts (http://geneatlas.roslin.ed.ac.uk, https://pheweb.org/UKB-SAIGE/) revealed that R1537C (A allele) is associated with specific

TABLE 1 Key resources used in this research.

Reagent or resource	Source	Identifier
Antibodies		
Rabbit monoclonal Anti-Gli3 antibody (1:1,000)	Abcam	Cat# ab181130
Rat monoclonal Anti-α-tubulin antibody (1:1,000)	Abcam	ab9267
Biotinylated anti-rabbit IgG antibody (1:2,000)	Vector Laboratories	BA-1000
Biotinylated anti-rat IgG antibody (1:2,000)	Vector Laboratories	BA-4000
Rabbit monoclonal Anti-Olig2 antibody (1:1,000)	Abcam	ab109186
Rat monoclonal Anti-GFP antibody (1:1,000)	Nakalai Tesque	04404-84
Anti-rat antibody Alexa-Fluor 488 conjugated (1:500)	Life Technologies	A11006
Anti-rabbit antibody Alexa-Fluor 594 conjugated (1:500)	Life Technologies	A11012
Bacterial and virus strains		
DH5α competent cells	Clontech	Cat# 9057
Chemicals, peptides, and recombinant proteins		
Doxycycline	Clontech	REF# 631311
Cas12a (Cpf1) protein	Integrated DNA Technologies	Cat# 10001272
BsmBI-v2	New England Biolab	R0739
BsmAI	New England Biolab	R0529
Critical commercial assays		
Dual-Luciferase Reporter Assay System	Promega	E1910
DNeasy Blood and Tissue Kit	QIAGEN	REF# 69504
RNeasy Mini Kit	QIAGEN	REF# 74104
In-Fusion HD Cloning Kit	Clontech	Cat# 639648
Vectastain Elite ABC Kit	Vector Laboratories	PK-6100
Chemi-Lumi One Super	Nacalai Tesque	Cat# 02230-30
Deposited data		
Original data sets	This paper: Mendeley Data	doi: 10.17632/mwdwkddfh8.1
Raw RNA-seq data of HEK293T cells	This paper: DDBJ	DRA01589
Experimental models: Cell lines		
Gli-reporter NIH3T3 cells	BPS Bioscience	Cat# 60409
HEK293T cells	RIKEN BRC Cell Bank	RBRC-RCB2202
HEK293 Tet-Off Advanced cell line	Clontech	Cat# 631152
GLI3 KO HAP-1	Horizon Genomics	HZGHC007467c021
Experimental models: Organisms/strains		
Mouse: $Gli3^{R1540C}$ (C57BL6/J)	This paper: Background strain is from Charles River Laboratories Japan	N/A
Mouse: $Gli3^{R1540C}$ (CD-1)	This paper: Background strain is from Japan SLC	N/A
Mouse $Gli3^{R1540Sfs}$ (CD-1)	This paper: Background strain is from Japan SLC	N/A
Fertilized chicken eggs (Gallus gallus)	Yamagishi, Japan	N/A

(Continued on following page)

TABLE 1 (*Continued*) Key resources used in this research.

Reagent or resource	Source	Identifier
Antibodies		
Oligonucleotides		
mGli3_R1540C_crRNA: CCACAGCTCCTCCCGTCTCACCAC	This paper: Integrated DNA Technologies	N/A
mGli3_R1540C_ssDNA: ACCAGCCTAATGTCAGGGGCCTTGAGCCCAAGTATTATTCAG AACCTTTCCCACAGCTCCTCCTGTCTCACCACTCCGCGGGCATCCCTCCCATTCCCA TCCCTATCCATGGGCACCACCAACA	This paper: Integrated DNA Technologies	N/A
Genotyping primer: mGli3_amplicon_fwd CGGTATCGATAAGCTGGTGTGCAGATTGATTG	Macrogen	N/A
Genotyping primer: mGli3_amplicon_rev ATTCGATATCAAGCTTCAGCAAAGAACTCA TATCC	Macrogen	N/A
Recombinant DNA		
pEGFPC3-hGli3	Addgene	#65435
pRL Renilla Luciferase Control Reporter Vector	Promega	
p8xGli-BS-delta51-LucII	RIKEN BRC DNA Bank	RDB08061
pcDNA3.1-His-Gli1	RIKEN BRC DNA Bank	RDB08063
pCMV-Gli3-Myc-DDK	ORIGENE	MR226591
pCAG-GLI3^{MH}	This study	N/A
pCAG-RB	Watanabe et al. (2011)	N/A
pCAG-GLI3^{R1537C}	This study	N/A
pCAG-GLI3^{MH}ΔRD	This study	N/A
pCAG-GLI3^{R1537C}ΔRD	This study	N/A
pTRE3G-NlucP	Addgene	#162595
pTRE3G-GLI3^{MH}NlucP	This study	N/A
pTRE3G-GLI3^{R1537C}NlucP	This study	N/A
pCAG-Gli3	This study	N/A
pCAG-Gli3^{R1540C}	This study	N/A
pBluescript II SK	Agilent Technology	Cat# 212205
Software and algorithms		
Excel (v16.54)	Microsoft	N/A
Prism 9 (v9.1.2)	GraphPad software	N/A
ImageJ (1.45s)	NIH, United States	https://imagej.nih.gov/ij/index.html
Adobe Photoshop 2021	Adobe	N/A
HISAT2 (v2.1.0)	Zhang et al. (2021)	https://daehwankimlab.github.io/hisat2/
StringTie (v 2.1.3b)	Shumate et al. (2022)	https://ccb.jhu.edu/software/stringtie/
Gene Ontology	The Gene Ontology Consortium	http://geneontology.org
g:Profiler tool	Raudvere et al. (2019)	https://biit.cs.ut.ee/gprofiler/gost
CHOPCHOP (v3)	Labun et al. (2019)	https://chopchop.cbu.uib.no
Human Phenotype Ontology	Kohler et al. (2021)	https://hpo.jax.org/app/

anatomical traits, such as anisotropy of the superior longitudinal fasciculus (p = 0.00038) waist-hip ratio (p = 0.00057), and other unspecified back disorders (p = 0.0000045), while the modern human variant (G allele) increases the risk of lethargy (p = 0.00058) and osteoarthritis (p = 0.00067). Although most of these associations did not pass statistical correction for multiple comparisons, these traits are linked with the predicted lifestyles of Neanderthals, suggesting that R1537C provided beneficial traits for extinct hominins. To distinguish these possibilities, further analyses are required to identify the biological effects of the variant in human development, as well as genetic and epigenetic modifiers that affect variant-dependent phenotypes.

Materials and methods

Animals

Male and female mice (CD-1 and C57BL6/J backgrounds) that were originally obtained from Japan SLC and Charles River Laboratories Japan were maintained in a 12 h dark/light cycle at the Experimental Animal Facility of Kyoto Prefectural University of Medicine. Noon of the day the vaginal plug was identified was designated as E0.5. Fertilized chicken eggs (*Gallus gallus*) were obtained from a local farm (Yamagishi, Japan) and incubated at 37.0°C ± 0.2°C. Embryonic stages were determined according to the Hamburger-Hamilton stages (Hamburger and Hamilton, 1951). All animal experiments were approved by the experimental animal committee of Kyoto Prefectural University of Medicine and were performed in accordance with the relevant guidelines (M2021–233, M2022-209, M2021-511, M2022-210, M2021-217, M2022-201).

Plasmids

Full-length human GLI3 and mouse Gli3 cDNAs were obtained from pEGFPC3-hGli3 [a gift from Aimin Liu, Addgene plasmid (Zeng et al., 2010)] and pCMV-Gli3-Myc-DDK (ORIGENE, MR226591), and then subcloned into the pCAG-RB vector by using an In-Fusion HD cloning kit. For construction of pCAG-GLI3^{R1537C} and pCAG-mGli3^{R1540C}, the 3' regions of GLI3 or mGli3 were replaced with PCR-amplified fragments containing c4609t (GLI3^{R1537C}) or c4618t (mGli3^{R1540C}), respectively. pCAG-GLI3^{MH}ΔRD and pCAG-GLI3^{R1537C}ΔRD were generated by subcloning the C-terminal region of GLI3^{MH} or GLI3^{R1537C} into the pCAGRB vector, according to the method of a previous report (Stamataki et al., 2005). For construction of pTRE-GLI3^{MH}-NLucP and pTRE-GLI3^{R1537C}-NLucP, coding sequences of GLI3^{MH} or GLI3^{R1537C} were subcloned into pTRE3G-NlucP [a gift from Masaharu Somiya, addgene plasmid (Somiya and Kuroda, 2021)]. All vectors were verified by sequencing.

Luciferase reporter assay

Gli-reporter NIH3T3 cells were transfected with pCAG-GLI3^{MH} or pCAG-GLI3^{R1537C} together with pTK-RL by using Lipofectamine 2000 (Thermo Fisher Scientific). To monitor Gli-dependent luciferase activity in HEK293T cells, p8xGli-BS-delta51-LucII (Sasaki et al., 1997) was transfected with other expression vectors. As a control condition, the pCAGRB empty vector was cotransfected with reporter vectors. For analysis of GLI1-dependent reporter activities, pcDNA3.1-His-Gli1 (Sasaki et al., 1999) was transfected with GLI3 expression vectors. Transfected cells were cultured in Dulbecco's modified Eagle's medium (high glucose, Nacalai Tesque) containing 10% fetal bovine serum and 1% penicillin and streptomycin (Fujifilm Wako Pure Chemical Corporation) for 24 h. For analysis of the degradation rates of GLI3^{MH} and GLI3^{R1537C}, pTRE-GLI3^{MH}-NLucP or pTRE-GLI3^{R1537C}-NLucP was transfected into the HEK293 Tet-Off Advanced cell line, and doxycycline was then added to the culture medium 12 h after transfection. Luciferase activity was examined with the Dual-Luciferase Reporter Assay System and analyzed with a luminometer (GENE LIGHT GL210A, Microtec, Inc.). All firefly luciferase values were normalized to Renilla luciferase activities. At least three biologically independent samples were analyzed in each experimental condition, and all experiments were confirmed by at least three technical replicates.

GLI3 KO cell line

A GLI3 knockout cell line (HZGHC007467c021, Horizon Genomics) was generated by manufacture's protocols. Briefly, 166 bp of bovine minisatellite genomic sequence was inserted into GLI3 genomic locus of HAP1 cells by CRISPR/Cas9 system. A frame-shift mutation with ectopic stop codons in exon 5 was confirmed by sanger sequencing. Parental cell line (WT HAP1) carries modern human type GLI3 variant (1540R). Sequence information of the cell line is available on Mendeley data.

Western blotting

HEK293T cells transfected with pCAG-GLI3^{MH}, pCAG-GLI3^{R1537C}, pCAG-mGli3, or pCAG-mGli3^{R1540C} were lysed in RIPA buffer (20 mM Tris, 150 mM NaCl, 1 mM EDTA, 1% Nonidet P40, 1% SDS, 0.1% deoxycholate, 1 mM NaF and protein inhibitor). GLI3 KO or WT HAP1 cells were directly lysed in RIPA buffer. and After electrophoresis, proteins were transferred to Poly Vinylidene Di-Fluoride (PVDF) membranes, blocked with Bullet Blocking One for Western blotting (Nacalai Tesque), and then incubated with anti-human GLI3 or anti-α-tubulin antibody. The membranes were further incubated with biotinylated anti-rabbit IgG or biotinylated anti-rat IgG antibody, followed by a Vectastain Elite ABC kit and developed with Chemi-Lumi One Super and analyzed with a luminescent image analyzer (LAS-2000, Fujifilm). For Western blotting with mouse brains, the cerebellar primordium of E17.5 mice were manually dissected and lysed in RIPA buffer.

In ovo electroporation

In ovo electroporation of developing chick embryos was performed according to a previous study (Stamataki et al., 2005). Briefly, a window

was opened in the shell of an egg, and then a small amount of DNA solution (less than 0.05 μL) was injected into the neural tube of E2 (HH stage 13–15) embryos with a fine glass needle. Needle-type electrodes (CUY200S, BEX) were placed on the neural tube and square electric pulses (28 V for 50 ms, 2 or 3 times) were applied to the thoracic neural tube with a pulse generator (CUY21 EDITII, BEX). After electroporation, the extraembryonic cavity was filled with sterilized Hank's balanced salt solution (HBSS, Nacalai Tesque) containing antibiotics (penicillin/streptomycin and gentamycin), and the window was sealed with parafilm. Electroporated embryos were incubated in an incubator at 37°C for 24–48 h.

Immunohistochemistry

Electroporated embryos were fixed with 4% paraformaldehyde dissolved in phosphate-buffered saline (PBS) at 4°C overnight. After PBS washes, the embryos were cryoprotected with a 20% sucrose solution and immersed in Tissue-Tek. The frozen samples were sectioned at a thickness of 20 μm using a cryostat (Leica CM 1850, Germany), and incubated with primary antibodies, including anti-Olig2 and anti-GFP antibodies. After washing, the sections were incubated with secondary antibodies, including Alexa-Fluor 488 or 594 conjugated anti-rat or anti-rabbit antibodies. Fluorescence images were captured with fluorescence microscopes (BX51, Olympus) equipped with a cooled CCD camera (DP80, Olympus). All captured images were processed with cell Sense standard (v.1.17, Olympus), ImageJ and Adobe Photoshop.

RNA-seq analyses

Total RNA was prepared from HEK293T cells transfected with pCAG-RB, pCAG-GLI3^{MH} or pCAG-GLI3^{R1537C} by using an RNeasy kit. To isolate total RNA from mouse tissue, thoracic mesenchymal tissue of E17.5 wild-type and 1540C mice was dissected and preserved in RNAlater until RNA extraction. Residual DNA was eliminated by DNase treatment. The quality and quantity of RNAs were assessed by using an Agilent Technologies 2100 Bioanalyzer or 2200 TapeStation (Agilent). The cDNA library was constructed using a TrueSeq Standard mRNA LT Sample Prep Kit according to the manufacturer's protocol (15031047 Rev. E) and sequenced on an Illumina platform and 101 bp paired-end reads were generated. The sequence data were mapped to a reference genome sequence (*Homo sapiens* GRCh38; NCBI_109.20200522 or *Mus musculus* GRCm38, GCA_000001635.2) with a splice-aware aligner (HISAT2 v 2.1.0). The transcripts were assembled by StringTie (v 2.1.3b) with aligned reads. GO enrichment analysis was performed based on Gene Ontology. A significant gene list was constructed by the g:Profiler tool.

SNP population genetics

The genetic population of rs35364414 (GLI3 4609G/A) was analyzed by Ensemble genome browser 108 (https://www.ensembl.org/index.html).

Mouse genome engineering

For generation of a point mutation in mouse Gli3 that corresponds to a Neanderthal GLI3 variant, genome edited mouse lines were established by CRISPR/Cas12a (Cpf1)-mediated homology directed repair (HDR). A crRNA sequence that targets mouse Gli3 4618c was designed by CHOPCHOP. We chose a target sequence with no off targets based on mouse genome information (mm10/GRCm38). As an HDR template for homologous recombination, single strand DNA (ssDNA) that carries a nucleotide substation (4618t) was designed by using the mouse Gli3 sequence.

Generation of genome edited mice

The cumulus complexes were isolated from superovulated female C57BL6/J mice treated with pregnant mare serum gonadotropin (PMSG) and human chronic gonadotropin (hCG), and then mixed with sperm taken from the epididymis of male C57BL6/J mice. After *in vitro* fertilization, the CRISPR/Cas12a solution containing Cpf1 protein (Integrated DNA Technology, Inc.), crRNA, and ssDNA were introduced into zygotes by electroporation (Genome Editor Plus. BEX, Tokyo, Japan). After electroporation, the zygotes were transferred into the oviduct of pseudopregnant CD-1 mice. Anesthesia was performed by intraperitoneal injection of medetomidine, midazolam and butorphanol. Genome-edited mice on the CD-1 background were generated by the *i*-GONAD method (Gurumurthy et al., 2019). Briefly, pregnant female mice (E0.75) were anesthetized with 2% isoflurane and the CRISPR/Cas12a solution was injected into the oviduct lumen. Then, square electric pulses were applied to the oviduct by using a pulse generator (super electroporator NEPA21, Nepa gene).

Genotyping of mice

Genomic DNA from embryonic or adult mouse tissue (skin or tail fragments) was prepared using a DNeasy Blood and Tissue kit. The DNA fragments containing the CRISPR/Cas12a target region were amplified by polymerase chain reaction (PCR). PCR fragments were digested by BsmBI for 1 h, and the restriction fragment length was determined by electrophoresis with 3% agarose. For determination of the edited sequences of candidate mouse lines, PCR amplicons were subcloned into the pBluescriptSK vector, and six to ten randomly selected clones were examined by Sanger sequencing. F0 mice heterozygous for the 4618c > t substitution (Gli3^{R1537C}) were propagated and used to generate homozygous mice.

Skeletal analyses

Embryonic and postnatal mice were collected (embryonic Day 16.5, postnatal Day 1, or Day 7) and dissected in phosphate buffered saline. The samples were fixed with 100% ethanol for 3 days and degreased by acetone overnight. Skeletal staining was

performed by Alcian blue and Alizarin red according to a standard protocol (Rigueur and Lyons, 2014). Sample images were captured by using the microscope (SZX7, Olympus) equipped with a cooled CCD camera (DP80, Olympus).

Image processing and analyses

Images of Western blotting were examined by using ImageJ. All captured images were processed with Adobe Photoshop 2021. Original Western blotting images were deposited in Mendeley Data.

Statistical analyses

For statistical analysis, at least three independent samples from each experimental group were compared. Comparisons between experimental groups were performed using Microsoft Excel and Prism 9. All data are presented as the mean ± SE. Statistical significance was determined using the two-tailed unpaired Student's t-test, ordinary one-way ANOVA with Tukey's multiple comparisons test, or two-way ANOVA with Sidak's multiple comparison test. Statistical analysis of differential gene expression conducted by RNAseq data was performed using fold change and the nbinomWald Test using the DESeq2 R package (Bioconductor) per comparison pair, and significant results were selected based on $|fc| \geq 1.5$ and nbinomWald Test with a raw p-value < 0.05.

Data availability statement

The datasets presented in this study can be found in online repositories. The names of the repository/repositories and accession number(s) can be found below: https://www.ddbj.nig.ac.jp/, DRA015189, https://www.ddbj.nig.ac.jp/, DRA015774, https://data.mendeley.com/datasets/mwdwkddfh8, 10.17632/mwdwkddfh8.2. Key resources used in this study is listed in Table 1.

Ethics statement

The animal study was approved by the Kyoto Prefectural University of Medicine Ethics Committee for Animal Experiments. The study was cunducted in accordance with the local legistration and institutional requirements.

Author contributions

AA and TN contributed to the experimental design, data collection, interpretation, and manuscript preparation. SO contributed to the generation and maintenance of mice carrying $GLI3^{R1540C}$. RN contributed to the collection and analysis of RNA-seq samples, HG and KO contributed to the acquisition of the reagents and interpretation. All authors contributed to the article and approved the submitted version.

Funding

This work was supported by Japanese Grants-In-Aid for Scientific Research (KAKENHI, 21H02591 to TN), the Koyanagi Foundation (to TN), the Ohsumi Frontier Science Foundation (to TN), and the Japanese Association of University Woman (JAUW) to AA.

Acknowledgments

We thank Drs. Ikuo K. Suzuki and Takuma Kumamoto for critically reading the manuscript and Ms. Kawami Misato and Ms. Mariko Yazaki for technical assistance.

Conflict of interest

The authors declare that the research was conducted in the absence of any commercial or financial relationships that could be construed as a potential conflict of interest.

Publisher's note

Supplementary material

The Supplementary Material for this article can be found online at: https://www.frontiersin.org/articles/10.3389/fcell.2023.1247361/full#supplementary-material

References

Alappat, S., Zhang, Z. Y., and Chen, Y. P. (2003). Msx homeobox gene family and craniofacial development. *Cell Res.* 13, 429–442. doi:10.1038/sj.cr.7290185

Asgari, S., Luo, Y., Akbari, A., Belbin, G. M., Li, X., Harris, D. N., et al. (2020). A positively selected FBN1 missense variant reduces height in Peruvian individuals. *Nature* 582, 234–239. doi:10.1038/s41586-020-2302-0

Cargill, M., Altshuler, D., Ireland, J., Sklar, P., Ardlie, K., Patil, N., et al. (1999). Characterization of single-nucleotide polymorphisms in coding regions of human genes. *Nat. Genet.* 22, 231–238. doi:10.1038/10290

Carroll, S. B. (2000). Endless forms: the evolution of gene regulation and morphological diversity. *Cell* 101, 577–580. doi:10.1016/s0092-8674(00)80868-5

Castellano, S., Parra, G., Sánchez-Quinto, F. A., Racimo, F., Kuhlwilm, M., Kircher, M., et al. (2014). Patterns of coding variation in the complete exomes of three Neandertals. *Proc. Natl. Acad. Sci. U. S. A.* 111, 6666–6671. doi:10.1073/pnas.1405138111

Chan, Y. F., Marks, M. E., Jones, F. C., Villarreal, G., Shapiro, M. D., Brady, S. D., et al. (2010). Adaptive evolution of pelvic reduction in sticklebacks by recurrent deletion of a Pitx1 enhancer. *Science* 327, 302–305. doi:10.1126/science.1182213

Chasman, D., and Adams, R. M. (2001). Predicting the functional consequences of non-synonymous single nucleotide polymorphisms: structure-based assessment of amino acid variation. *J. Mol. Biol.* 307, 683–706. doi:10.1006/jmbi.2001.4510

Demurger, F., Ichkou, A., Mougou-Zerelli, S., Le Merrer, M., Goudefroye, G., Delezoide, A. L., et al. (2015). New insights into genotype-phenotype correlation for GLI3 mutations. *Eur. J. Hum. Genet.* 23, 92–102. doi:10.1038/ejhg.2014.62

Dong, X., Pi, Q., Yuemaierabola, A., Guo, W., and Tian, H. (2021). Silencing LINC00294 restores mitochondrial function and inhibits apoptosis of glioma cells under hypoxia via the miR-21-5p/CASKIN1/cAMP Axis. *Oxid. Med. Cell Longev.* 2021, 8240015. doi:10.1155/2021/8240015

Enard, W., Przeworski, M., Fisher, S. E., Lai, C. S. L., Wiebe, V., Kitano, T., et al. (2002). Molecular evolution of FOXP2, a gene involved in speech and language. *Nature* 418, 869–872. doi:10.1038/nature01025

Filvaroff, E. H., Guillet, S., Zlot, C., Bao, M., Ingle, G., Steinmetz, H., et al. (2002). Stanniocalcin 1 alters muscle and bone structure and function in transgenic mice. *Endocrinology* 143, 3681–3690. doi:10.1210/en.2001-211424

Garcia-Martinez, D., Bastir, M., Gómez-Olivencia, A., Maureille, B., Golovanova, L., Doronichev, V., et al. (2020). Early development of the Neanderthal ribcage reveals a different body shape at birth compared to modern humans. *Sci. Adv.* 6, eabb4377. doi:10.1126/sciadv.abb4377

Gokhman, D., Mishol, N., de Manuel, M., de Juan, D., Shuqrun, J., Meshorer, E., et al. (2020). Reconstructing denisovan anatomy using DNA methylation maps. *Cell* 180, 601. doi:10.1016/j.cell.2020.01.020

Gokhman, D., Mishol, N., de Manuel, M., de Juan, D., Shuqrun, J., Meshorer, E., et al. (2019). Reconstructing denisovan anatomy using DNA methylation maps. *Cell* 179, 180–192. doi:10.1016/j.cell.2019.08.035

Green, R. E., Krause, J., Briggs, A. W., Maricic, T., Stenzel, U., Kircher, M., et al. (2010). A draft sequence of the Neandertal genome. *Science* 328, 710–722. doi:10.1126/science.1188021

Greer, C., Bhakta, H., Ghanem, L., Refai, F., Linn, E., and Avella, M. (2021). Deleterious variants in genes regulating mammalian reproduction in Neanderthals, Denisovans and extant humans. *Hum. Reprod.* 36, 734–755. doi:10.1093/humrep/deaa347

Gurumurthy, C. B., Sato, M., Nakamura, A., Inui, M., Kawano, N., Islam, M. A., et al. (2019). Creation of CRISPR-based germline-genome-engineered mice without *ex vivo* handling of zygotes by i-GONAD. *Nat. Protoc.* 14, 2452–2482. doi:10.1038/s41596-019-0187-x

Hamburger, V., and Hamilton, H. L. (1951). A series of normal stages in the development of the chick embryo. *J. Morphol.* 88, 49–92. doi:10.1002/jmor.1050880104

Hoekstra, H. E., and Coyne, J. A. (2007). The locus of evolution: evo devo and the genetics of adaptation. *Evolution* 61, 995–1016. doi:10.1111/j.1558-5646.2007.00105.x

Kang, S., Graham, J. M., Jr., Olney, A. H., and Biesecker, L. G. (1997). GLI3 frameshift mutations cause autosomal dominant Pallister-Hall syndrome. *Nat. Genet.* 15, 266–268. doi:10.1038/ng0397-266

Kohler, S., Gargano, M., Matentzoglu, N., Carmody, L. C., Lewis-Smith, D., Vasilevsky, N. A., et al. (2021). The human phenotype Ontology in 2021. *Nucleic Acids Res.* 49, D1207–D1217. doi:10.1093/nar/gkaa1043

Kvon, E. Z., Kamneva, O. K., Melo, U. S., Barozzi, I., Osterwalder, M., Mannion, B. J., et al. (2016). Progressive loss of function in a limb enhancer during snake evolution. *Cell* 167, 633–642. doi:10.1016/j.cell.2016.09.028

Labun, K., Montague, T. G., Krause, M., Torres Cleuren, Y. N., Tjeldnes, H., and Valen, E. (2019). CHOPCHOP v3: expanding the CRISPR web toolbox beyond genome editing. *Nucleic Acids Res.* 47, W171–W174. doi:10.1093/nar/gkz365

Levi, G., Narboux-Neme, N., and Cohen-Solal, M. (2022). DLX genes in the development and maintenance of the vertebrate skeleton: implications for human pathologies. *Cells* 11, 3277. doi:10.3390/cells11203277

Maricic, T., Helmbrecht, N., Riesenberg, S., Macak, D., Kanis, P., Lackner, M., et al. (2021). Comment on "Reintroduction of the archaic variant of NOVA1 in cortical organoids alters neurodevelopment. *Science* 374, eabi6060. doi:10.1126/science.abi6060

Matissek, S. J., and Elsawa, S. F. (2020). GLI3: a mediator of genetic diseases, development and cancer. *Cell Commun. Signal* 18, 54. doi:10.1186/s12964-020-00540-x

Mc, L. A., and Michie, D. (1958). Factors affecting vertebral variation in mice. 4. Experimental proof of the uterine basis of a maternal effect. *J. Embryol. Exp. Morphol.* 6, 645–659.

Meyer, M., Kircher, M., Gansauge, M. T., Li, H., Racimo, F., Mallick, S., et al. (2012). A high-coverage genome sequence from an archaic Denisovan individual. *Science* 338, 222–226. doi:10.1126/science.1224344

Mora-Bermudez, F., Kanis, P., Macak, D., Peters, J., Naumann, R., Xing, L., et al. (2022). Longer metaphase and fewer chromosome segregation errors in modern human than Neanderthal brain development. *Sci. Adv.* 8, eabn7702. doi:10.1126/sciadv.abn7702

Naruse, I., Ueta, E., Sumino, Y., Ogawa, M., and Ishikiriyama, S. (2010). Birth defects caused by mutations in human GLI3 and mouse Gli3 genes. *Congenit. Anom. (Kyoto)* 50, 1–7. doi:10.1111/j.1741-4520.2009.00266.x

Orlowski, J., and Grinstein, S. (1997). Na+/H+ exchangers of mammalian cells. *J. Biol. Chem.* 272, 22373–22376. doi:10.1074/jbc.272.36.22373

Pinson, A., Xing, L., Namba, T., Kalebic, N., Peters, J., Oegema, C. E., et al. (2022). Human TKTL1 implies greater neurogenesis in frontal neocortex of modern humans than Neanderthals. *Science* 377, eabl6422. doi:10.1126/science.abl6422

Protas, M. E., Hersey, C., Kochanek, D., Zhou, Y., Wilkens, H., Jeffery, W. R., et al. (2006). Genetic analysis of cavefish reveals molecular convergence in the evolution of albinism. *Nat. Genet.* 38, 107–111. doi:10.1038/ng1700

Prufer, K., de Filippo, C., Grote, S., Mafessoni, F., Korlević, P., Hajdinjak, M., et al. (2017). A high-coverage neandertal genome from vindija cave in Croatia. *Science* 358, 655–658. doi:10.1126/science.aao1887

Prufer, K., Racimo, F., Patterson, N., Jay, F., Sankararaman, S., Sawyer, S., et al. (2014). The complete genome sequence of a Neanderthal from the Altai Mountains. *Nature* 505, 43–49. doi:10.1038/nature12886

Qiu, J., Zhou, S., Cheng, W., and Luo, C. (2020). LINC00294 induced by GRP78 promotes cervical cancer development by promoting cell cycle transition. *Oncol. Lett.* 20, 262. doi:10.3892/ol.2020.12125

Raudvere, U., Kolberg, L., Kuzmin, I., Arak, T., Adler, P., Peterson, H., et al. (2019). g: Profiler: a web server for functional enrichment analysis and conversions of gene lists (2019 update). *Nucleic Acids Res.* 47, W191–W198. doi:10.1093/nar/gkz369

Reich, D., Green, R. E., Kircher, M., Krause, J., Patterson, N., Durand, E. Y., et al. (2010). Genetic history of an archaic hominin group from Denisova Cave in Siberia. *Nature* 468, 1053–1060. doi:10.1038/nature09710

Reilly, P. F., Tjahjadi, A., Miller, S. L., Akey, J. M., and Tucci, S. (2022). The contribution of Neanderthal introgression to modern human traits. *Curr. Biol.* 32, R970–R983. doi:10.1016/j.cub.2022.08.027

Renard, E., Chéry, C., Oussalah, A., Josse, T., Perrin, P., Tramoy, D., et al. (2019). Exome sequencing of cases with neural tube defects identifies candidate genes involved in one-carbon/vitamin B12 metabolisms and Sonic Hedgehog pathway. *Hum. Genet.* 138, 703–713. doi:10.1007/s00439-019-02015-7

Rengasamy, P., and Padmanabhan, R. R. (2004). Experimental studies on cervical and lumbar ribs in mouse embryos. *Congenit. Anom. (Kyoto)* 44, 156–171. doi:10.1111/j.1741-4520.2004.00029.x

Rigueur, D., and Lyons, K. M. (2014). Whole-mount skeletal staining. *Methods Mol. Biol.* 1130, 113–121. doi:10.1007/978-1-62703-989-5_9

Ronshaugen, M., McGinnis, N., and McGinnis, W. (2002). Hox protein mutation and macroevolution of the insect body plan. *Nature* 415, 914–917. doi:10.1038/nature716

Sankararaman, S., Mallick, S., Patterson, N., and Reich, D. (2016). The combined landscape of denisovan and neanderthal ancestry in present-day humans. *Curr. Biol.* 26, 1241–1247. doi:10.1016/j.cub.2016.03.037

Sasaki, H., Hui, C., Nakafuku, M., and Kondoh, H. (1997). A binding site for Gli proteins is essential for HNF-3beta floor plate enhancer activity in transgenics and can respond to Shh *in vitro*. *Development* 124, 1313–1322. doi:10.1242/dev.124.7.1313

Sasaki, H., Nishizaki, Y., Hui, C., Nakafuku, M., and Kondoh, H. (1999). Regulation of Gli2 and Gli3 activities by an amino-terminal repression domain: implication of Gli2 and Gli3 as primary mediators of Shh signaling. *Development* 126, 3915–3924. doi:10.1242/dev.126.17.3915

Shumate, A., Wong, B., Pertea, G., and Pertea, M. (2022). Improved transcriptome assembly using a hybrid of long and short reads with StringTie. *PLoS Comput. Biol.* 18, e1009730. doi:10.1371/journal.pcbi.1009730

Skov, L., Coll Macià, M., Sveinbjörnsson, G., Mafessoni, F., Lucotte, E. A., Einarsdóttir, M. S., et al. (2020). The nature of Neanderthal introgression revealed by 27,566 Icelandic genomes. *Nature* 582, 78–83. doi:10.1038/s41586-020-2225-9

Somiya, M., and Kuroda, S. (2021). Reporter gene assay for membrane fusion of extracellular vesicles. *J. Extracell. Vesicles* 10, e12171. doi:10.1002/jev2.12171

Stamataki, D., Ulloa, F., Tsoni, S. V., Mynett, A., and Briscoe, J. (2005). A gradient of Gli activity mediates graded Sonic Hedgehog signaling in the neural tube. *Genes Dev.* 19, 626–641. doi:10.1101/gad.325905

Tessadori, F., Duran, K., Knapp, K., Fellner, M., and Smithson, S. (2022). Recurrent *de novo* missense variants across multiple histone H4 genes underlie a neurodevelopmental syndrome. *Am. J. Hum. Genet.* 109, 750–758. doi:10.1016/j.ajhg.2022.02.003

Trujillo, C. A., Rice, E. S., Schaefer, N. K., Chaim, I. A., Wheeler, E. C., Madrigal, A. A., et al. (2021). Reintroduction of the archaic variant of NOVA1 in cortical organoids alters neurodevelopment. *Science* 371, eaax2537. doi:10.1126/science.aax2537

Veistinen, L. K., Mustonen, T., Hasan, M. R., Takatalo, M., Kobayashi, Y., Kesper, D. A., et al. (2017). Regulation of calvarial osteogenesis by concomitant de-repression of GLI3 and activation of IHH targets. *Front. Physiol.* 8, 1036. doi:10.3389/fphys.2017.01036

Veistinen, L., Takatalo, M., Tanimoto, Y., Kesper, D. A., Vortkamp, A., and Rice, D. P. C. (2012). Loss-of-Function of Gli3 in mice causes abnormal frontal bone morphology and premature synostosis of the interfrontal suture. *Front. Physiol.* 3, 121. doi:10.3389/fphys.2012.00121

Vortkamp, A., Gessler, M., and Grzeschik, K. H. (1991). GLI3 zinc-finger gene interrupted by translocations in Greig syndrome families. *Nature* 352, 539–540. doi:10.1038/352539a0

Wang, B., Fallon, J. F., and Beachy, P. A. (2000). Hedgehog-regulated processing of Gli3 produces an anterior/posterior repressor gradient in the developing vertebrate limb. *Cell* 100, 423–434. doi:10.1016/s0092-8674(00)80678-9

Wang, C., Ruther, U., and Wang, B. (2007). The Shh-independent activator function of the full-length Gli3 protein and its role in vertebrate limb digit patterning. *Dev. Biol.* 305, 460–469. doi:10.1016/j.ydbio.2007.02.029

Watanabe, K., Takebayashi, H., Bepari, A. K., Esumi, S., Yanagawa, Y., and Tamamaki, N. (2011). Dpy19l1, a multi-transmembrane protein, regulates the radial migration of glutamatergic neurons in the developing cerebral cortex. *Development* 138, 4979–4990. doi:10.1242/dev.068155

Wen, X., Lai, C. K., Evangelista, M., Hongo, J. A., de Sauvage, F. J., and Scales, S. J. (2010). Kinetics of hedgehog-dependent full-length Gli3 accumulation in primary cilia and subsequent degradation. *Mol. Cell Biol.* 30, 1910–1922. doi:10.1128/MCB.01089-09

Werner, T., Koshikawa, S., Williams, T. M., and Carroll, S. B. (2010). Generation of a novel wing colour pattern by the Wingless morphogen. *Nature* 464, 1143–1148. doi:10.1038/nature08896

Zeberg, H., Dannemann, M., Sahlholm, K., Tsuo, K., Maricic, T., Wiebe, V., et al. (2020). A neanderthal sodium channel increases pain sensitivity in present-day humans. *Curr. Biol.* 30, 3465–3469. doi:10.1016/j.cub.2020.06.045

Zeng, H., Jia, J., and Liu, A. (2010). Coordinated translocation of mammalian Gli proteins and suppressor of fused to the primary cilium. *PLoS One* 5, e15900. doi:10.1371/journal.pone.0015900

Zhang, Y., Park, C., Bennett, C., Thornton, M., and Kim, D. (2021). Rapid and accurate alignment of nucleotide conversion sequencing reads with HISAT-3N. *Genome Res.* 31, 1290–1295. doi:10.1101/gr.275193.120

Zhou, X., Lv, L., Zhang, Z., Wei, S., and Zheng, T. (2020). LINC00294 negatively modulates cell proliferation in glioma through a neurofilament medium-mediated pathway via interacting with miR-1278. *J. Gene Med.* 22, e3235. doi:10.1002/jgm.3235

Zhou, H., Kim, S., Ishii, S., and Boyer, T. G. (2006). Mediator modulates Gli3-dependent Sonic hedgehog signaling. *Mol. Cell Biol.* 26, 8667–8682. doi:10.1128/MCB.00443-06